Received: 14 July 2017 | Revised: 14 August 2017 | Accepted: 1 October 2017

DOI: 10.1002/chir.22778

SPECIAL ISSUE ARTICLE

WILEY

Transition dipole coupling modeling of optical activity enhancements in macromolecular protein systems

Jiří Průša[1,2] | Petr Bouř[1,2]

[1] Institute of Organic Chemistry and Biochemistry, Academy of Sciences, Prague, Czech Republic

[2] University of Chemistry and Technology, Prague, Czech Republic

Correspondence
Petr Bouř, Institute of Organic Chemistry and Biochemistry, Flemingovo náměstí 2, Prague 6, 16610, Czech Republic.
Email: bour@uochb.cas.cz

Funding information
Grant Agency of the Czech Republic, Grant/Award Number: 15-09072S; Ministry of Education, Grant/Award Number: LTC17012

Abstract

Optical activity of regular molecular assemblies, such as protein fibrils or nucleic acid condensates, is often significantly stronger than for isolated molecules. Previous modeling suggested that this may be caused by the ordered quasi-periodic structure and a long-order synchronization of chromophore excitations. In the present study, we briefly review this phenomenon and investigate some aspects on simple models related to protein vibrational optical activity. The transition dipole coupling (TDC) model is used to generate vibrational circular dichroism (VCD) and Raman optical activity (ROA) spectra. While a linear arrangement of chromophores produced relatively simple couplet intensity patterns, a richer band structure was predicted for planar geometries. A stacking of β-sheet planes has been identified as another powerful source of the enhancement. The results do not completely reproduce experimental observations but are consistent with them and confirm that chiroptical methods may be extremely useful to study aggregation of chiral molecules.

KEYWORDS

circular dichroism, enhancement of optical activity, protein spectra, Raman optical activity, transition dipole coupling

1 | INTRODUCTION

Chiroptical methods exploring different interaction of left and right circularly polarized light with chiral molecules established as useful tools to study molecules and their assemblies, such as sugars, nucleic acids, and proteins. An interesting phenomenon, enhancement of the chirality in molecular aggregates, was first observed in the electronic circular dichroism (ECD) of nucleic acids. By condensation of DNA strands at high salt concentrations, ECD intensity significantly increased when compared, for example, with standard B-DNA spectrum.[1] Later, this so called ψ-type circular dichroism ("psi" for polymer and salt-induced) was observed in a range of DNA samples.[1-13] An analogous observation was reported in the infrared region for vibrational circular dichroism (VCD).[14]

For proteins, ECD enhancement in such an extent is not known. However, a closely related "exciton coupling" has often been pointed out as a principal mechanism leading to large spectral intensities in α-helical structures.[15-17]

More spectacular effects for proteins have been observed in the vibrational region. Formation of fibrous aggregates, such as β-amyloidal plugs related to a wide variety of neurodegenerative diseases, is often accompanied by a large enhancement of the VCD signal.[18-21] A typical example is shown in Figure 1 for lysozyme. The "fibrillation" of the native protein is accompanied by much smaller changes in the absorption spectrum. A very good indicator of the enhancement is thus also the dimensionless dissymmetry factor (*g*, the ratio of the VCD signal

[This article is part of the Special Thematic Issue in Memory of Ettore Castiglioni: Chiroptical Spectroscopy: Instrumentation, Experimental Aspects and Application. See the first articles for this special issue previously published in Volumes 29:9, 29:10, 29:11, and 29:12. More special articles will be found in this issue as well as in those to come.]

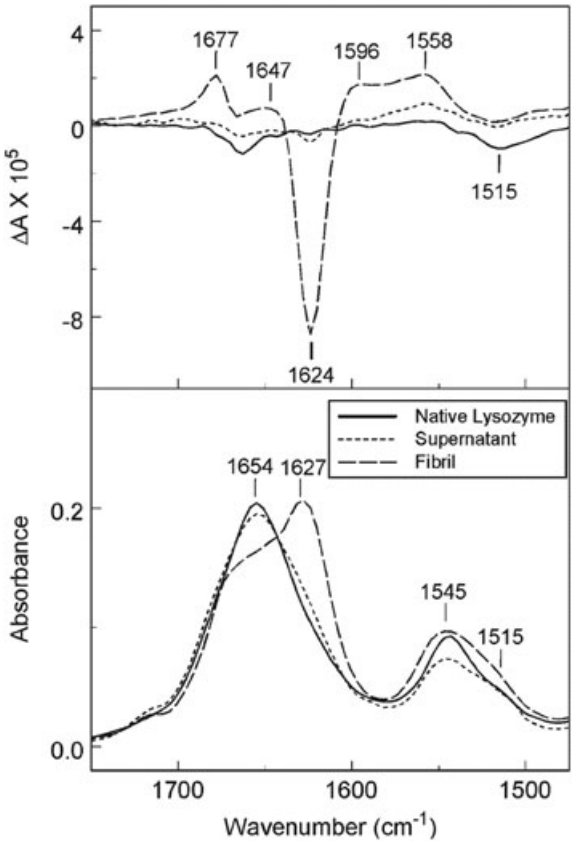

FIGURE 1 Enhanced VCD of lysozyme fibrils (top, dashed line) and corresponding absorption spectra (bottom). Spectra of the soluble native protein are plotted by the dotted and full lines. Reprinted with permission from Ma. S. et al. *J. Am. Chem. Soc.* **2007**, *129*, 12364. Copyright American Chemical Society

to the absorption). For the lysozyme, it rose from about 5×10^{-5} to ~4×10^{-4}.

Because the "fibrils" often do not crystallize and give rather mediocre NMR signal, the vibrational spectra thus potentially provide a welcome window allowing one to monitor protein structure.[22] The enhancement is also favorable for the VCD spectroscopy itself, as the technique is traditionally restricted by the weakness of the phenomenon and difficulties associated with measurement of artifact-free spectra.[23] Large dissymmetry factors may cut down the measurement times, from hours to minutes.

Explorations of analogous exciton-like enhancements of Raman optical activity (ROA) are still at the beginning. Raman optical activity measurements of condensed macromolecular systems are very difficult. The enhancement may appear as an experimental artifact, and vice versa.[24] Yet some studies such as that on polyproline strands of variable length[25] showed that mechanical coupling between neighboring residues does lead to a significant dependence of some ROA bands on peptide length. Another interesting ROA enhancement phenomenon was lately observed for astaxanthin (carotenoid dye) aggregates, sometimes exhibiting huge signal in comparison with monomer spectra.[26] This phenomenon, however, was explained by resonance effects,[26,27] i.e., it is most probably not related to the "mechanical" exciton coupling of the chromophores modeled in the present study.

Because of the size of the aggregates, theoretical foundations of the chirality enhancement are rather incomplete. A polarizability theory relating the phenomenon to a long range coupling of the chromophore[28-30] helped to explain some variety in ψ-ECD of DNA samples.[3,31,32] At the present study, we use the transition dipole coupling (TDC) approximation to look at dependence of VCD and ROA spectra on geometry of model systems. Transition dipole coupling has been previously used to successfully model CD enhancement in nucleic acids[33] and VCD patterns of protein β-sheet structures including fibrils.[34-36] Depending on macroscopical orientation of β-sheet planes reasonable approximation to experimental spectra was obtained, although still not reproducing observable dissymmetry factors and detailed splitting of VCD bands.[36] In the present study, a larger variation of the geometries is explored, some of them providing a more realistic pattern. We also find interesting the enhancement predicted for ROA spectra, although not confirmed by an experiment so far.

2 | MATERIALS AND METHODS

2.1 | Transition dipole coupling

Within the transition dipole coupling (TDC) model,[34,37,38] extensive molecular systems can be treated relatively cheaply in terms of computer time and memory. The chromophores (for example, the protein C═O groups) are represented by interacting dipoles. The potential between dipoles $\boldsymbol{\mu}_j$ and $\boldsymbol{\mu}_i$ is

$$V_{ij} = \frac{\boldsymbol{\mu}_i \cdot \boldsymbol{\mu}_j \mathbf{r}_{ij}^2 - 3\boldsymbol{\mu}_i \cdot \mathbf{r}_{ij} \boldsymbol{\mu}_j \cdot \mathbf{r}_{ij}}{\mathbf{r}_{ij}^5}, \quad (1)$$

where $\mathbf{r}_{ij}$ is the vector connecting dipole positions and dots are used for scalar products. Atomic units are used throughout. The positions are somewhat arbitrary. For the CO molecule-like modeling the middle of the C═O bond was used; for amides, the amide I and amide II vibrational dipoles were put in geometrical centers of the HNCO atoms. Solving the Schrödinger equation in a basis of monoexcited states ("excitons") leads to diagonalization of the Hamiltonian matrix with off-diagonal elements equal to V_{ij} and diagonal ones equal to transition energies ε_i. In the first approximation, the transition energies are the same for same chromophores. From the eigenvectors $\mathbf{c}^\lambda$ and eigenvalues (energies) of the Hamiltonian, we can calculate spectral intensities. The resultant transition electric and magnetic dipole moments are

$$\boldsymbol{\mu}_\lambda = \sum_{i=1}^{N} c_i^\lambda \ \boldsymbol{\mu}_i \tag{2}$$
$$\mathbf{m}_\lambda = \frac{i}{2}\sum_{i=1}^{N} \varepsilon_i c_i^\lambda \mathbf{r}_i \times \boldsymbol{\mu}_i,$$

respectively, where N is number of the chromophores and $\mathbf{r}_i$ are chromophore position vectors. Similarly, for Raman and ROA transition polarizabilities (electric dipole-electric dipole, $\boldsymbol{\alpha}$, electric dipole-magnetic dipole, $\mathbf{G'}$, and electric dipole-electric quadrupole, $\mathbf{A}$), we get

$$\boldsymbol{\alpha}_\lambda = \sum_{i=1}^{N} c_i^\lambda \alpha_i, \tag{3}$$
$$\mathbf{G}_\lambda^{'} = \sum_{i=1}^{N} c_i^\lambda \ \mathbf{G}_i^{'},$$
$$\mathbf{A}_\lambda = \sum_{i=1}^{N} c_i^\lambda \ \mathbf{A}_i.$$

The TDC model for ROA is then closely related to the group-polarizability approximation.[39] We neglect mutual polarization of the chromophores as this has a rather minor effect on the spectra.[40,41] However, origin-dependence of $\mathbf{G'}$ and $\mathbf{A}$ has to be taken into account. The tensors in the common origin (COM) depend on those in the local origin (LOC, at $\mathbf{r}_i$) as[39]

$$\boldsymbol{\alpha}_i(COM) = \boldsymbol{\alpha}_i(LOC), \tag{4}$$
$$\mathbf{G}_i^{'}(COM) = \mathbf{G}_i^{'}(LOC) - \frac{i}{2}\mathbf{r}_i \times \boldsymbol{\alpha}_i,$$
$$A_{i,\alpha\beta\gamma}(COM) = A_{i,\alpha\beta\gamma}(LOC) + \frac{3}{2}\left(\alpha_{i\alpha\gamma} r_{i\beta} + \alpha_{i\alpha\beta} r_{i\gamma}\right) + \delta_{\beta\gamma}\sum_{\varepsilon}^{3} \alpha_{i\alpha\varepsilon} r_{i\varepsilon}.$$

The local parts of $\mathbf{G'}$ and $\mathbf{A}$ were neglected.

Model systems included one-dimensional arrays of dipoles, and arrays assembled into a plane and a "twisted" plane (**A**-**C**, Figures 2 and 3). In the array, the dipoles were perpendicular to the propagation axis z, regularly spaced and rotated. A tilt toward the axis had no effect on the enhancement and was then not considered. In the planes, the dipole helical arrays were separated by 3.5 Å. B3LYP/6-31G** vibrational parameters calculated for carbon monoxide were used.

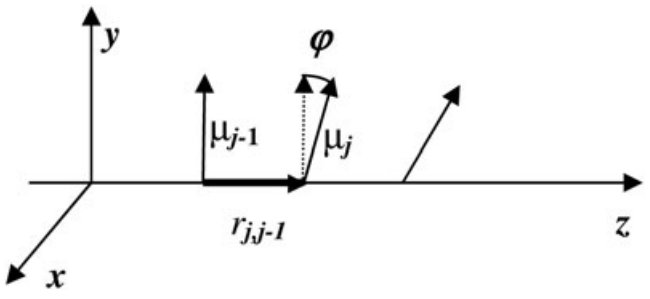

FIGURE 2 The dipole array characterized by mutual rotation (φ) and distance ($r_{j,j-1}$)

In addition to the mono-dipole carbon monoxide-like systems, B3LYP/6-31G** amide I and II mode parameters of N-methylacetaldehyde were used to model planar systems of amide groups **1** to **4** (Figure 3, lower part). Their local geometries (distances) were inspired by typical x-ray protein fibril structures from the protein data bank (http://www.rcsb.org/), in particular by the human islet amyloid polypeptide.[42] The two basic (regular, **F**, and perturbed, **T**) units were propagated regularly, using translations and rotations only. The B3LYP/6-31G**amide I frequency was scaled to 1650 cm^{-1} to better correspond to experimental spectra.

In the middle, "fibril-like" amide (HNCO) group planes **1** to **4** are displayed. They were constructed either from flat (**F**) or perturbed (**T**) 7-amide units and mimic a parallel β-sheet. An example of overlap of the flat model, HNCO atoms in red, with x-ray fibril geometry[42] is given at the bottom.

3 | RESULTS AND DISCUSSION

3.1 | The TDC model

Before discussing larger systems, we document basic properties of the TDC model on a model pair of formamide molecules in Figure 4. We also want to document the ability of TDC to model ROA intensities, which has been discussed rather rarely.[43] The input spectral parameters for monomer (transition frequencies, dipoles $\boldsymbol{\mu}_i$ and polarizabilities $\boldsymbol{\alpha}_i$) were calculated for optimized monomer geometry at the BPW/6-31G** level of theory; the molecules were co-planar, rotated by 45°, and separated by 5 Å. Three monomer transitions (at 2861, 1784, and 1574 cm^{-1}) were included. One can see that the TDC results closely reproduce the DFT ones. As follows from the theory,[39] the chiral spectra (VCD and ROA) are conservative for TDC, i.e., integral of the spectral intensities is zero. Note that the TDC approximation is justified for this case when the interaction potential between vibrations localized on the chromophores is well described by formula 1. Also, local quadrupole and magnetic terms are negligible compared to the global ones obtained from Equations 2 and 4. For shorter distances, electron transfer may occur and the TDC results may significantly deviate from the "exact" (in this case DFT) results as discussed elsewhere.[44] In the work of Measey and Schweitzer-Stenner,[36] for example, a more advanced variety of the TDC model is used, replacing the electrostatic potential

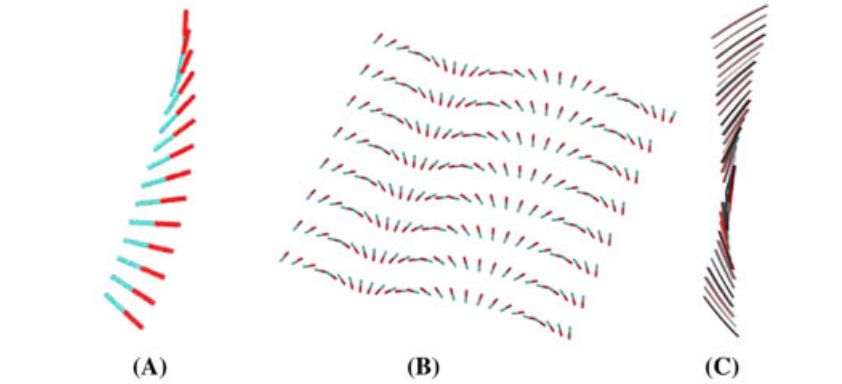

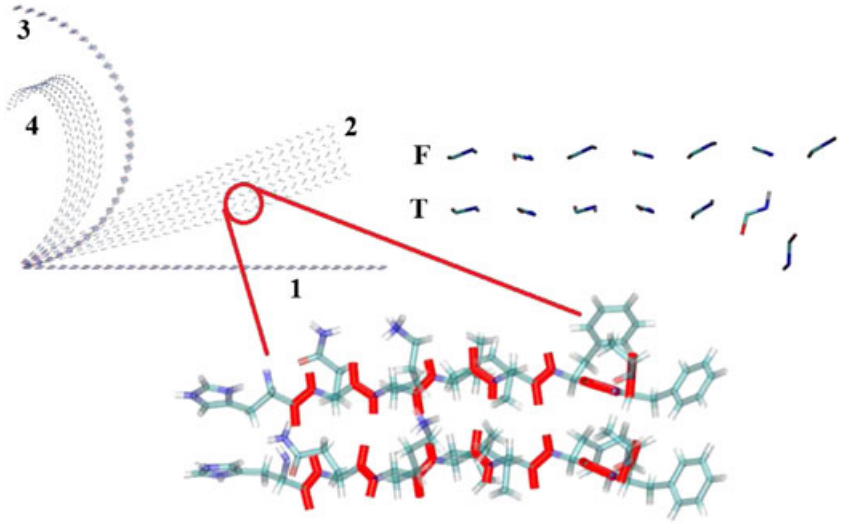

FIGURE 3 Example geometries of (**A**) one-dimensional dipole array, and (**B**) planar and (**C**, a plane seen from a side) "twisted plane" arrangement. **B** is composed of one-dimensional arrays in a plane, while in **C** the arrays are incrementally twisted by 0.4 °. The dipoles are spaced 3.5 Å the arrays separated by 4 Å. In the middle, "fibril-like" amide (HNCO) group planes **1-4** are displayed. They were constructed either from flat (**F**) or perturbed (**T**) 7-amide units and mimic a parallel b-sheet. An example of overlap of the flat model, HNCO atoms in red, with x-ray fibril geometry[42] is given at the bottom

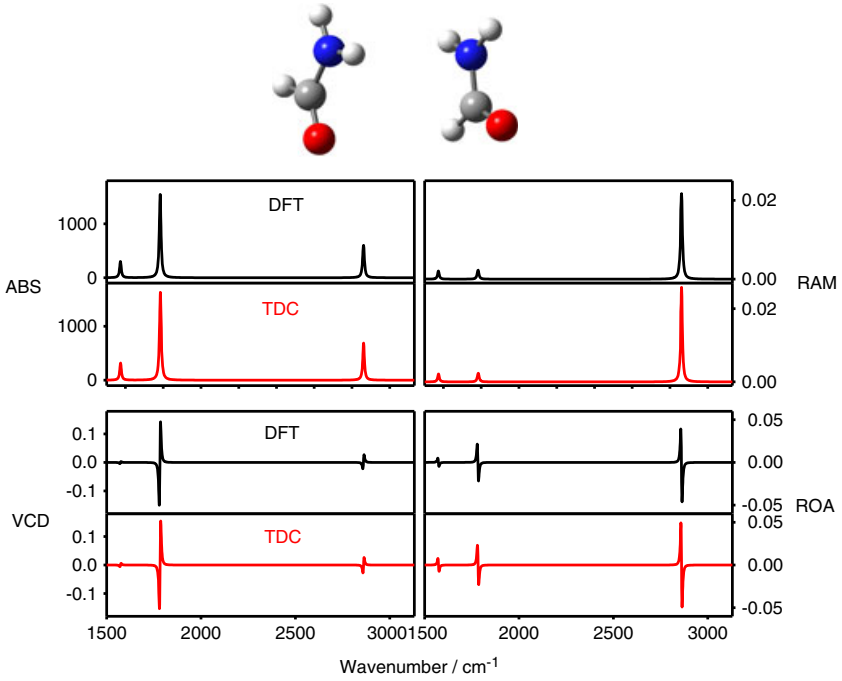

FIGURE 4 Absorption, VCD, Raman, and ROA spectra of a formamide dimer obtained by the DFT and TDC models

between neighboring amides by a constant term. For our case, the TDC approximation seems reasonable to reproduce the main spectral features and inter-chromophore interactions.

3.2 | One-dimensional array

For the one-dimensional array of identical dipoles (Figures 2 and 3A), the dipole magnitude and the twist angle were varied. The mutual dipole distance (3.5 Å) was fixed. Other input parameters (polarizability and transition frequency) corresponded to values calculated for carbon oxide (CO) at the B3LYP/6-31G** level of theory. Dependencies of VCD dissymmetry factor g and circular intensity difference (*CID*, ratio of ROA and Raman intensities) on the dipole magnitude and the twist were obtained for 40 dipoles. The working formulae for g and *CID* (caption of Figure 5) are slightly different from the usual ones,[39] to describe observable intensities for non-resolved transitions.[45]

As expected, larger values of the transition dipole cause larger coupling and consequently larger g values, except for non-chiral geometries ($\varphi = 0°$ and 180°) and angles implying zero dipole-dipole interaction ($\varphi = 90°$ and 270°) (Figure 5). We can also note the 2π (360°) periodicity of *CID*, while the g values repeat already with π periodicity, which is related to a symmetry "breaking" by the transition dipole moment generating the VCD intensities: Unlike the dipole moment, polarizability components (eg, α_{xx}) important for ROA do not change sign under rotation by 180°.

At the lower two graphs in Figure 5, relative enhancements are plotted, defined as ratios of g or *CID* obtained for the 40-mer to values calculated for a dimer. Clearly, for small dipole moments ($\mu < \sim 0.2$) the vibrational coupling is small and the relative enhancement is close to one (no enhancement, indistinguishable from zero at the adopted scale). For larger dipoles, the enhancement rises up to ~30 but only for nearly parallel geometries (φ close to 0° or 180°). This is consistent with previous VCD studies where the signal enhancement has been observed exclusively for semi-planar β-sheet geometries.[18-21] For ROA, analogous enhancement experiments are not known to us, although some data suggest that similar phenomenon can occur here, too (cf. Supporting Information in Yamamoto and Watarai[24]). We can also see that largest enhancements ($g/g_2 = CID/CID_2 = 30$) occur for ROA in a narrower angular intervals ($\varphi = 0° \ldots 15°$, etc) than for VCD ($\varphi \sim 0° \ldots 30°$), which makes experimental observations of ROA enhancement less likely.

3.3 | Planar array arrangement

Arrangement of the one-dimensional dipole arrays (helices) into the plane or slightly twisted plane (structures **B**-**C**) did not bring significant signal enhancement.

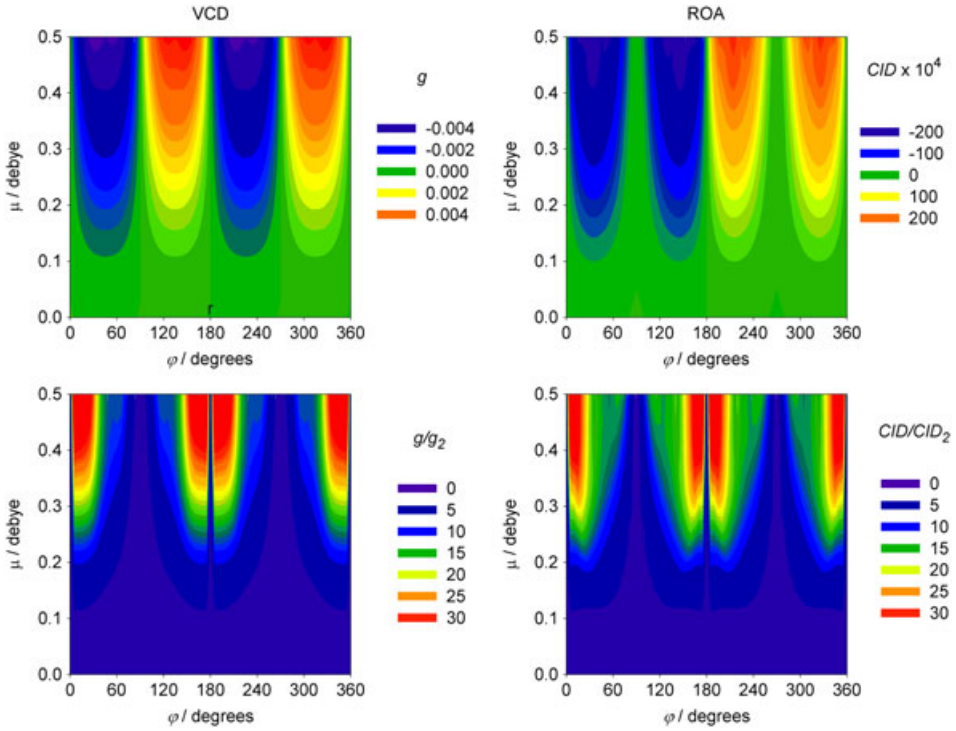

FIGURE 5 TDC simulation of VCD and ROA intensities for one-dimensional array of 40 identical dipoles. The dissymmetry factor (g) was obtained by integration of the VCD ($\Delta\varepsilon$) and absorption (ε) intensities ($g = \int(\omega - \omega_0)\ \Delta\varepsilon d\omega / \int \omega\varepsilon d\omega$), ω_0 is the central position of the VCD couplet. Similarly, the circular intensity difference (*CID*) was obtained from ROA ($\Delta I = I_R - I_L$) and Raman ($I = I_R + I_L$) intensities as $CID = \int(\omega - \omega_0)\Delta I d\omega / \int \omega I d\omega$. At the bottom two panels enhancements obtained by division of g and *CID* by values obtained for dimer are plotted

However, the spectra became more structured. This is shown in Figure 6 for $\varphi = 10°$ and $\mu = 0.4$ D. For the one-dimensional structure (**A**) both the absorption and VCD intensity accumulates around 2570 cm^{-1}. As pointed out previously,[33] this corresponds to the longest wavelength phonon-like mode within the array where the dipoles vibrate in phase. Mutual interaction of the arrays in the planes perturbs this mechanism; while the absorption is still concentrated around 2400 cm^{-1}, VCD intensity becomes spread more evenly across all vibrational modes. The flat and twisted planes (**B** and **C**) give virtually the same spectra. The ROA and Raman spectra behaved in the same way as VCD and absorption and are not shown. For this combination of φ and μ the *g*-factor ($\Delta\varepsilon/\varepsilon = 10^{-3}$) is rather high; as follows from Figure 4 even larger values can be achieved for larger dipoles providing a stronger coupling.

g-factors and *CID*s of model planes (**B** and **C**) as dependent on the twist and dipole magnitudes are plotted in Figure 7. Qualitatively, there is a little difference between the flat **B** and distorted **C** planes. For both cases the *g*-factors rises for $\varphi \to 0$ and $\varphi \to 180°$. Unlike for the array, significant *g* enhancements occur only for a very limited areas of the (μ, φ) plane, in particular for $\varphi \to 0$ and $\varphi \to 180°$. This is qualitatively similar for *CID* (lower part of Figure 7), where, however, the largest values occur around $\varphi = 120°$.

3.4 | "Amide" planes

The systems of amide group atoms was designed to mimic more realistic protein systems. The planes **1** to **4**, using the regular or perturbed units (**F** or **T**, Figure 3) provided spectra plotted in Figure 8. The dissymmetry factor for the regular "flat" unit (~5×10^{-5}) is smaller than for the system built with the **T** fragments ($g = 1.3 \times 10^{-4}$), which are about the values seen in the previous planar models outside the "enhancement" regions (**B**-**C**, Figure 7). The

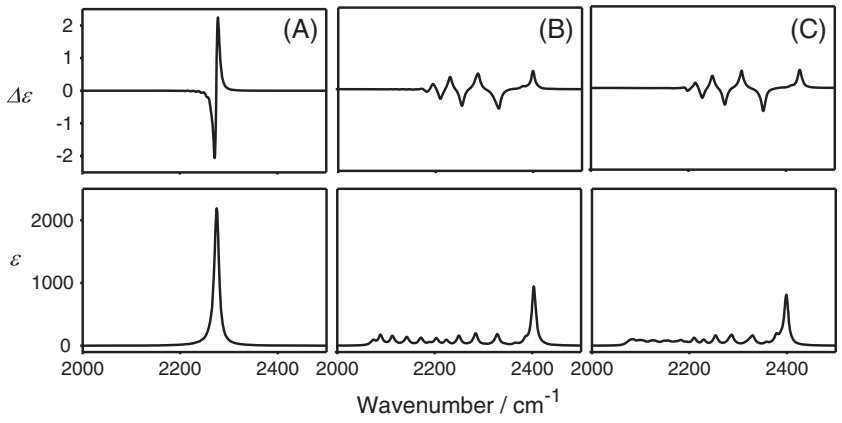

FIGURE 6 VCD ($\Delta\varepsilon$) and absorption (ε) spectra of the one- (**A**) and two (**B** and **C**) dimensional model dipole systems from Figure 3

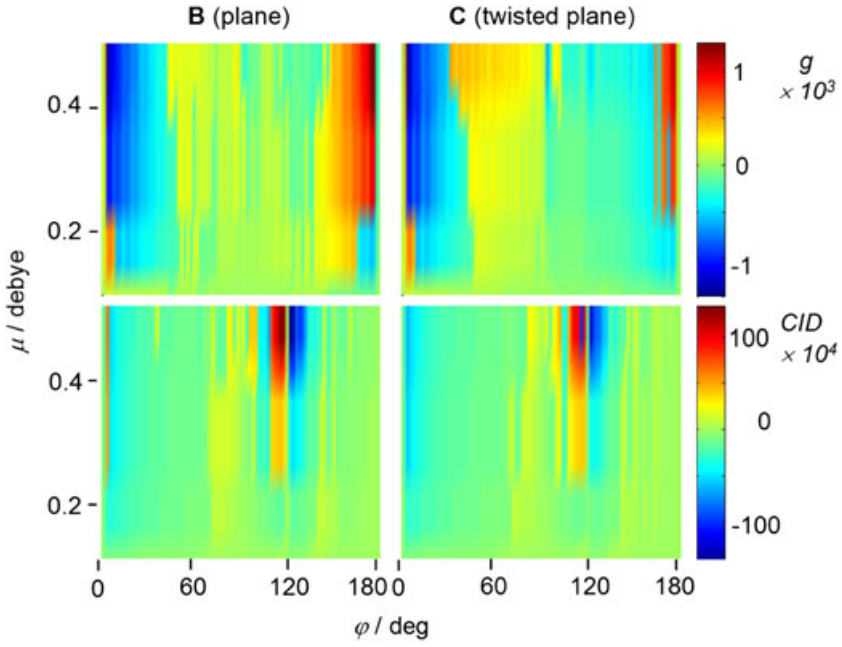

FIGURE 7 Dependence of the *g* (top) and *CID* (bottom) factors of the model planes **B** and **C** on the twist angle within the linear threads and magnitude of the dipole moment. Here, the *g* and *CID* factors were determined from spectral maxima ($\Delta\varepsilon_{max}/\varepsilon_{max}$, etc)

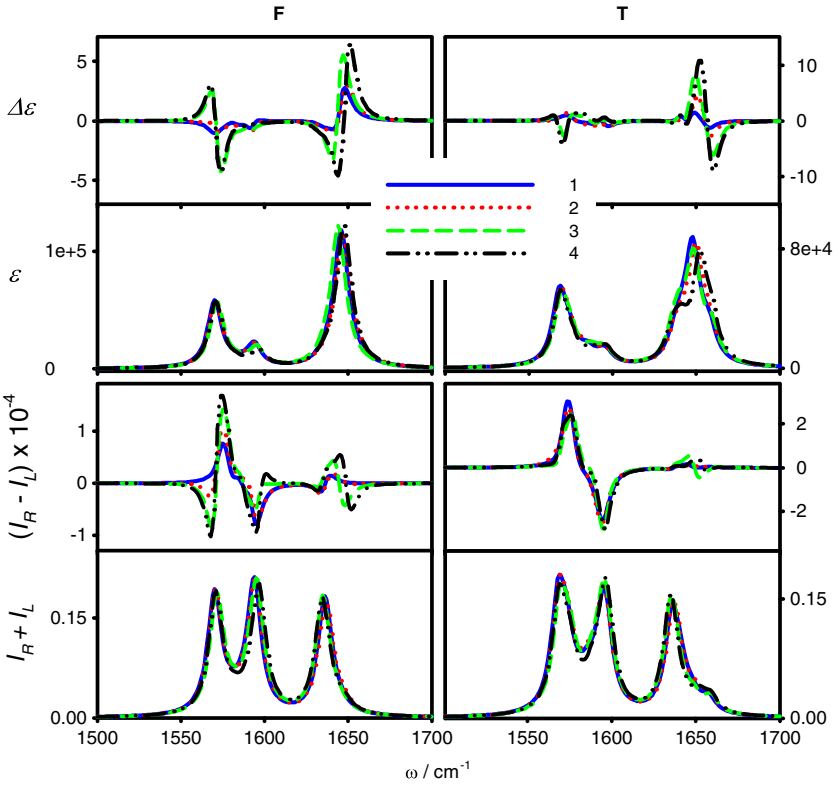

FIGURE 8 VCD, absorption, ROA, and Raman spectra of the amide planar structures (**1**-**4** plane types, **F** and **T** propagated unit, cf Figure 3)

F-model provides a larger amide II VCD (at ~1570 cm^{-1}), the **T** structure has a larger maximal amide I VCD signal (~1650 cm^{-1}) and gives an opposite sense of the couplet. Detailed spectra thus depend both on the "macroscopic" plane shape (cf. types **1** to **4**) and local chromophore structure (**F** or **T**). This is consistent with previous VCD fibril measurements revealing a remarkable variability of spectral shapes with respect to studied systems.[19,20,22] However, the theoretical *g*-factors seem to be quite small compared to maximal values observed experimentally (~10^{-2}-10^{-3}, e.g., Figure 1). In Figure 8, systems composed from 32 units are simulated; nevertheless, the *g*-factor is nearly independent of their number (not shown).

The ROA and Raman spectra (bottom of Figure 8) to a large degree behave as the VCD and absorption ones. Only relative peak intensities are different. While the main absorption amide I band is centered at 1645 cm^{-1}, maximal Raman intensity is shifted left, to ~1636 cm^{-1}. In both Raman and ROA spectra, the amide II signal is also more pronounced than for amide I; in particular, for the **T**-system, amide I ROA is quite small.

In experimental Raman spectra of β-sheet proteins (e.g., Baumruk and Keiderling[46] and Kessler et al[47]), the intense amide I component is higher in frequency than for ROA, which is not correctly predicted by the TDC model. This can be attributed to incomplete description of the in-strand CO stretching mode coupling by the electrostatic potential.[37] Similarly, the predicted relatively strong amide II signal is nearly invisible in Raman experiment.

The simulation thus does cannot reproduce detailed spectral features, but confirms that the planar arrangement of the chromophores provides an additional splitting of the amide bands compared to the one-dimensional chain, and that VCD and ROA shapes are able to reflect a longer-distance order of the chromophores, in our case the differently deformed planes **1** to **4**. On the other hand, building planar systems alone (without plane stacking) from the one-dimensional chromophore arrays does not seem to lead to significant chirality enhancements.

3.5 | Multi-layer amide systems

As found before, VCD intensity of twisted parallel β-sheet planes may be sometimes nearly independent of their distance *d*.[35,36] This may sound surprising; within the TDC model the dipole-dipole potential (1) and thus the energy-splitting quickly diminishes, being proportional to d^{-3}. On the other hand, each dipole in one plane can interact with "infinite" number of dipoles in the other one (in a large-plane limit). In addition, the magnetic dipole (Equation 2) responsible for VCD and the **G′** and **A** tensors (Equation 4) responsible for ROA are roughly proportional to the inter-chromophore distance, which can also counter-balance the fainting energy splitting.

This phenomenon is confirmed by the present simulations where we varied the planar distances, twists, and sizes. In the upper panels of Figure 9, we can see that both the *g* and *CID* factors do not dramatically fall off when the

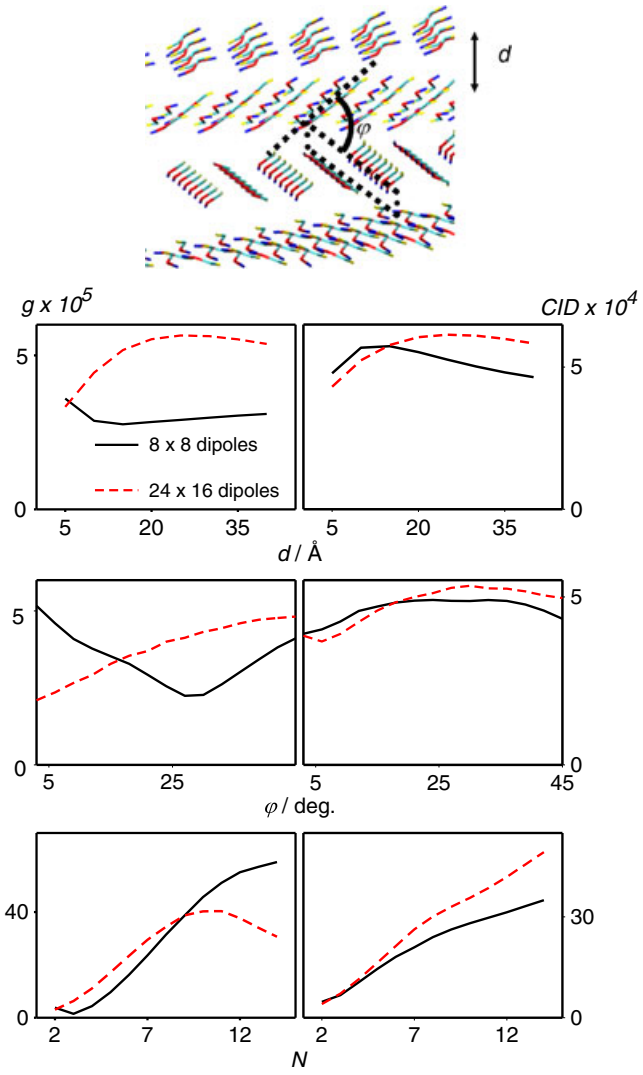

FIGURE 9 Small (8 × 8 amides) and larger (16 × 24) stacked and twisted amide planes, dependencies of the *g* and *CID* factors on the distance *d* (for $N = 2$ and $\varphi = 10°$), twist of the neighboring planes φ (for $N = 2$ and $d = 4$ Å), and the number of stacked planes (for $d = 4$ Å and $\varphi = 10°$)

distance between the planes increases. For the larger planes (16 × 24 amides) maxima are achieved at $d = 32$ Å. For the smaller plane (8 × 8 amides) the dependence of *g* on *d* is exceptional in having a minimum instead of maximum, at $d = 5$ Å.

For two planes, the results are thus qualitatively same as in previous works, where only a modest decrease[35] or increase[36] of the *g*-factor with the distance was found.

g and *CID* are also relatively insensitive to the twist angle (middle panels of Figure 9). This somewhat contrasts with the dependencies on the twist angle in the one-dimensional structures (cf Figures 5 and 7), but one has to realize that the amide planes are already chiral themselves; the inter-plane twist introduces just another perturbation.

The most interesting with respect to the long-order chirality enhancement is the dependence of *g* and *CID* on the number of stacked planes (bottom panels in Figure 9). Very large enhancements, of the order of 10 and more, can be achieved if measured against a 1-2 planar system. This is a trivial consequence of the relative independence of the chiral signal on the distance between two planes: for *N* stacked planes there are $N \times (N\text{-}1)/2$ inter-plane interactions. If these cause the optical activity, the signal thus can grow even as $\sim N^2$. The simulated dependencies are more complicated; the maximum of *g* at $N = 10$ (dashed line) even indicates that the planar stacking can even result to a signal cancelation. Nevertheless, the enhancements due to the plane stacking are quite impressive and may help to explain many events observable experiments involving molecular optical activity.

3.6 | Relation to experimental spectra

Clearly, the TDC modeling presented above is neither tailored to particular protein structure nor it can be used for a band-by-band analysis of an experiment, such as that shown in Figure 1. Nevertheless, it allows us to better understand the observations. The coupling of chromophores and consequent long-range synchronization of their vibrations clearly appear as important enhancement factors of optical activity. Two-dimensional planar structures (e.g., in Figures 6 and 8) provided a richer band splitting than the couplet typical for one-dimensional chains; such splitting is frequently visible in the amide I region of enhanced VCD of protein fibrils.[21] The predicted enhancement potential of the plane stacking explains many observations, such as sensitivity of measured signal to fibril size and their macroscopic twist.[18,48] Finally, the predicted enhancement in ROA of protein aggregates remains to be verified; so far, experimental data are scarce[24] and measurements very complicated.[49,50]

4 | CONCLUSION

We performed relatively simple TDC computations allowing us to systematically investigate the dependence of VCD and ROA spectra of model dipolar systems on the geometry. Although the simulations are not directly comparable to experiment in terms of band to band assignment, they provide a realistic basis for understanding the link between optical activity and structure of larger protein aggregates. The linear dipole arrays exhibited significant chirality enhancements, perhaps surprisingly most occurring for very small twist angles. The planar systems provided more complex dependencies and also more realistic band splitting with respect to previously observed spectra

of protein fibrils but did not add much to the overall chirality. Finally, the planar stacking of the chromophores has been identified as the most significant factor responsible for the observable enhancements. At the same time, we realize the limits of the current computational approach and further simulations are needed in the future to fully understand optical activity of aggregated proteins.

ACKNOWLEDGMENTS

The work was supported by the Grant Agency of the Czech Republic (15-09072S) and Ministry of Education (LTC17012).

ORCID

Petr Bouř http://orcid.org/0000-0001-8469-1686

REFERENCES

1. Lerman LS. A transition to a compact form of DNA in polymer solutions. *Proc Natl Acad Sci U S A*. 1971;68(8):1886-1890.
2. Jordan CF, Lerman LS, Venable JH. Structure and circular dichroism of DNA in concentrated polymer solutions. *Nature New Biol*. 1972;236(64):67-70.
3. Evdokimov YM, Platonov AL, Tikhonenko AS, Varshavsky YM. A compact form of double-stranded DNA in solution. *FEBS Lett*. 1972;23(2):180-184.
4. Evdokimov YM, Pyatigorskaya TL, Kadikov VA, et al. A compact form of double-stranded RNA in solutions containing poly(ethyleneglycol). *Nucleic Acids Res*. 1976;3(6):1533-1547.
5. Gosule LC, Schellman JA. Compact form of DNA induced by spermidine. *Nature*. 1976;259:333-335.
6. Haynes M, Garrett RA, Gratzer WB. Structure of nucleic acid-poly base complexes. *Biochemistry*. 1970;9(22):4410-4416.
7. Zacharias W, Martin JC, Wells RD. Condensed form of (dG-dC)n X (dG-dC)n as an intermediate between the B- and Z-type conformations induced by sodium acetate. *Biochemistry*. 1983;22(10):2398-2405.
8. Gersanovski D, Colson P, Houssier C, Fredericq E. Terbium($^{3+}$) as a probe of nucleic acids structure. Does it alter the DNA conformation in solution? *Biochim Biophys Acta*. 1985;824(4):313-323.
9. Cowman MK, Fasman GD. Circular dichroism analysis of mononucleosome DNA conformation. *Proc Natl Acad Sci U S A*. 1978;75(10):4759-4763.
10. Fasman GD, Schaffhausen B, Goldsmith L, Adler A. Conformational changes associated with f-1 histone-deoxyribonucleic acid complexes. Circular dichroism studies. *Biochemistry*. 1970;9(14):2814-2822.
11. Liao LW, Cole RD. Differences among subfractions of H1 histone in their interactions with linear and superhelical DNA. *Circular dichroism J Biol Chem*. 1981;256(13):6751-6755.
12. Khadake JR, Rao MR. DNA- and chromatin-condensing properties of rat testes H1a and H1t compared to those of rat liver H1bdec; H1t is a poor condenser of chromatin. *Biochemistry*. 1995;34(48):15792-15801.
13. Mura CV, Stollar BD. Interactions of H1 and H5 histones with polynucleotides of B- and Z-DNA conformations. *Biochemistry*. 1984;23(25):6147-6152.
14. Andrushchenko V, Leonenko Z, Cramb D, van de Sande H, Wieser H. Vibrational CD (VCD) and atomic force microscopy (AFM) study of DNA interaction with Cr^{3+} ions: VCD and AFM evidence of DNA condensation. *Biopolymers*. 2001;61(4):243-260.
15. Woody RW. Improved calculation of the nπ* rotational strength in polypeptides. *J Chem Phys*. 1968;49(11):4797-4806.
16. Woody RW. The exciton model and the circular dichroism of polypeptides. *Monatsh Chem*. 2005;136:347-366.
17. Johnson WC. Analyzing protein circular dichroism spectra for accurate secondary structures. *Proteins*. 1999;35:307-312.
18. Fulara A, Lakhani A, Wójcik S, Nieznańska H, Keiderling TA, Dzwolak W. Spiral superstructures of amyloid-like fibrils of polyglutamic acid: an infrared absorption and vibrational circular dichroism study. *J Phys Chem B*. 2011;115:11010-11016.
19. Kurouski D, Kar K, Wetzel R, Dukor RK, Lednev IK, Nafie LA. Levels of supramolecular chirality of polyglutamine aggregates revealed by vibrational circular dichroism. *FEBS Lett*. 2013;578(11):1638-1643.
20. Kurouski D, Dukor RK, Lu X, Nafie LA, Lednev IK. Spontaneous inter-conversion of insulin fibril chirality. *Chem Commun*. 2012;48:2837-2839.
21. Ma S, Cao X, Mak M, et al. Vibrational circular dichroism shows unusual sensitivity to protein fibril formation and development in solution. *J Am Chem Soc*. 2007;129:12364-12365.
22. Tobias F, Keiderling TA. Role of side chains in β-sheet self-assembly into peptide fibrils. IR and VCD spectroscopic studies of glutamic acid-containing peptides. *Langmuir*. 2016;32(18):4653-4661.
23. Nafie LA, Dukor RK. The Use of Dual Polarization Modulation in Vibrational Circular Dichroism Spectroscopy. In: Hicks JM, ed. *The Physical Chemistry of Chirality, ACS Symposium Series*. New York: Oxford University Press; 2000.
24. Yamamoto S, Watarai H. Raman optical activity study on insulin amyloid and prefibril intermediate. *Chirality*. 2012;24(2):97-103.
25. Profant V, Baumruk V, Li X, Šafařík M, Bouř P. Tracking of the polyproline folding by density functional computations and Raman optical activity spectra. *J Phys Chem B*. 2011;115:15079-15089.
26. Dudek M, Zajac G, Kaczor A, Baranska M. Aggregation-induced resonance Raman optical activity (AIRROA) and time-dependent helicity switching of astaxanthin supramolecular assemblies. *J Phys Chem B*. 2016;120:7807-7814.
27. Nafie LA. Theory of resonance Raman optical activity: the single electronic state limit chem. *Phys*. 1996;205(3):309-322.
28. Keller D, Bustamante C. Theory of the interaction of light with large inhomogeneous molecular aggregates. *I Absorption J Chem Phys*. 1986;84(6):2961-2971.

29. Keller D, Bustamante C. Theory of the interaction of light with large inhomogeneous molecular aggregates. 2. Psi-type circular-dichroism. *J Chem Phys*. 1986;84(6):2972-2980.
30. Kim MH, Ulibarri L, Keller D, Maestre MF, Bustamante C. The psi-type circular-dichroism of large molecular aggregates. 3. Calculations. *J Chem Phys*. 1986;84(6):2981-2989.
31. Evdokimov YM, Akimenko NM, Glukhova NE, Tikhonenko AS, Varshavsky YM. Production of the compact form of double-stranded DNA in solution in the presence of poly(ethylene glycol). *Mol Biol (USSR) (transl)*. 1972;7:124-132.
32. Widom J, Baldwin RL. Cation-induced toroidal condensation of DNA studies with $Co^{3+}(NH_3)_6$. *J Mol Biol*. 1980;144(4):431-453.
33. Andrushchenko V, Bouř P. Circular dichroism enhancement in large DNA aggregates simulated by a generalized oscillator model. *J Comput Chem*. 2008;29:2693-2703.
34. Schweitzer-Stenner R. Secondary structure analysis of polypeptides based on an excitonic coupling model to describe the band profile of amide I′ of IR, Raman, and vibrational circular dichroism spectra. *J Phys Chem B*. 2004;108(43):16965-16975.
35. Welch WRW, Kubelka J, Keiderling TA. Infrared, vibrational circular dichroism, and Raman spectral simulations for β-sheet structures with various isotopic labels, interstrand, and stacking arrangements using density functional theory. *J Phys Chem B*. 2013;117(36):10343-10358.
36. Measey T, Schweitzer-Stenner R. Vibrational circular dichroism as a probe of fibrillogenesis: the origin of the anomalous intensity enhancement of amyloid-like fibrils. *J Am Chem Soc*. 2011;133(4):1066-1076.
37. Kubelka J, Kim J, Bouř P, Keiderling TA. Contribution of transition dipole coupling to amide coupling in IR spectra of peptide secondary structures. *Vib Spectrosc*. 2006;42:63-73.
38. Moore WH, Krimm S. Transition dipole coupling in amide I modes of βpolypeptides. *Proc Natl Acad Sci U S A*. 1975;72(12):4933-4935.
39. Barron LD. *Molecular Light Scattering and Optical Activity*. Cambridge, UK: Cambridge University Press; 2004.
40. Yamamoto S, Li X, Ruud K, Bouř P. Transferability of various molecular property tensors in vibrational spectroscopy. *J Chem Theory Comput*. 2012;8(3):977-985.
41. Yamamoto S, Bouř P. On the limited precision of transfer of molecular optical activity tensors. *Collect Czech Chem Commun*. 2011;76(5):567-583.
42. Nielsen JT, Bjerring M, Jeppesen MD, et al. Unique identification of supramolecular structures in amyloid fibrils by solid-state NMR spectroscopy. *Angew Chem Int Ed*. 2009;48(12):2118-2121.
43. Polavarapu PL, Nafie L. Vibrational optical activity: comparison of theoretical and experimental results for (+)-(3R)-methylcyclohexanone. *J Chem Phys*. 1980;73(4):1567-1575.
44. Bouř P, Keiderling TA. Computational evaluation of the coupled oscillator model in the vibrational circular dichroism of selected small molecules. *J Am Chem Soc*. 1992;114:9100-9105.
45. Bouř P, Tam CN, Wang B, Keiderling TA. Rotationally resolved magnetic vibrational circular dichroism. Experimental spectra and theoretical simulation for diamagnetic molecules. *Mol Phys*. 1996;87:299-318.
46. Baumruk V, Keiderling TA. Vibrational circular dichroism of proteins in H_2O solution. *J Am Chem Soc*. 1993;115:6939-6942.
47. Kessler J, Kapitán J, Bouř P. First-principles predictions of vibrational Raman optical activity of globular proteins. *J Phys Chem Lett*. 2015;6(16):3314-3319.
48. Dzwolak W, Surmacz-Chwedoruk W, Babenko V. Conformational memory effect reverses chirality of vortex-induced insulin amyloid superstructures. *Langmuir*. 2013;29:365-370.
49. Blanch EW, Morozova-Roche LA, Cochran DAE, Doig AJ, Hecht L, Barron LD. Is polyproline II helix the killer conformation? A Raman optical activity study of the amyloidogenic prefibrillar intermediate of human lysozyme. *J Mol Biol*. 2000;301:553-563.
50. Kessler J, Yamamoto S, Bouř P. Establishing the link between fibril formation and Raman optical activity spectra of insulin. *Phys Chem Chem Phys*. 2017;19:13614-13621.

How to cite this article: Průša J, Bouř P. Transition dipole coupling modeling of optical activity enhancements in macromolecular protein systems. *Chirality*. 2018;30:55–64. https://doi.org/10.1002/chir.22778